Available online at www.sciencedirect.com
ScienceDirect
Trans. Nonferrous Met. Soc. China 28(2018) 1298−1310
Transactions of Nonferrous Metals Society of China
www.tnmsc.cn

Microstructural and mechanical behavior of blended powder semisolid formed Al7075/B_4C composites under different experimental conditions

A. JAVDANI, A. H. DAEI-SORKHABI

Department of Mechanical Engineering, Tabriz Branch, Islamic Azad University, Tabriz, Iran

Received 17 May 2017; accepted 19 December 2017

Abstract: This work aimed to fabricate B_4C reinforced aluminum matrix composites via blended powder semisolid forming that is an implementation of the benefits of semisolid forming to the powder metallurgy. Al7075 elements were incrementally added to ethanol solution under mechanical mixing. Al7075 constituents and B_4C particles were blended in a high energy ball mill. Cold compacted Al7075/B_4C blends were pressed at semisolid state. The effects of the size of the matrix (20, 45 and 63 μm), reinforcing volume fraction (5%, 10% and 20%) and semisolid compaction pressure (50 and 100 MPa) on the morphology, microstructure, density, hardness, compression and bending strength were thoroughly analyzed. Experimental results revealed that the highest microstructural uniformity was achieved when large B_4C particles (45 μm) were distributed within the small particles (20 μm) of the matrix phase. Composites with matrix particles larger than reinforcing phase indicated agglomerations in loadings more than 10% (volume fraction). Agglomerated regions resisted against penetration of the liquid phase to the pores and lowered the density and strength of these composites. Composites with 20 μm Al7075 and 20% (volume fraction) 45 μm B_4C powder pressed under 100 MPa exhibited the highest values of hardness (HV 190) and compressive strength (336 MPa).

Key words: blended powder; mechanical alloying; semisolid forming; B_4C; aluminum matrix composite

1 Introduction

Conventional engineering materials have limitations for some features in hardness, strength, density etc. Composite materials give the automotive, aerospace, and marine industry the opportunity to utilize reinforcing materials in different volume fractions. Metal matrix composites are known as materials that fulfill mechanical and physical requirements in a wide range of engineering applications. Among metal matrix composites, aluminum is widely used as matrix because of its low density, high specific strength, easy manufacturing, and high resistance to wear [1]. Particles, fibers and dispersoids are used to reinforce aluminum matrix. In composites reinforced with hard ceramic particles, it is possible to control mechanical, thermal, and tribological properties through determining reinforcing amount, size and distribution in the matrix phase [2]. Widely used conventional particles are SiC and Al_2O_3. Boron carbide is one of the reinforcements used in metal matrix composites reinforced with particles [3,4]. Boron carbide is harder and lighter than silicon carbide and alumina ceramics [5]; it has excellent thermal and chemical resistance and is also used in making bullet proof vests, armor tank and nuclear power plants [6].

Mechanical properties of the metal matrix composites are a function of production methods. Inspection of the published scientific result reveals that various manufacturing methods have been developed to manufacture aluminum matrix composites (AMCs), such as casting [7,8], semisolid forming [9], friction stir processing [10,11], and powder metallurgy [12]. Powder metallurgy affords the uniform distribution of reinforcing particles within the matrix. Effects of segregation and intermetallic compounds are less in this process [13]. However, the final products need post-processes such as machining [14]. In casting, reinforcing particles are added to a molten matrix. The major drawback of this method is the sedimentation of the reinforcing particles, which significantly influences the uniform distribution of the reinforcing particles within the matrix and lowers the quality of the final product [15]. In addition, this is carried out at high temperatures and needs more energy [16]. In semisolid forming methods, reinforcing particles are added to a semisolid matrix. The problem of

Corresponding author: A. H. DAEI-SORKHABI; E-mail: amirsorkhabi@iaut.ac.ir
DOI: 10.1016/S1003-6326(18)64767-3

sedimentation is partly dealt with in this way, but since the semisolid matrix has a high viscosity, the mixing process in high solid fractions may encounter some difficulties [16]. Therefore, in the industrial production of metal matrix composites, a method that can maintain the advantages of casting, semisolid forming, and powder metallurgy processes is of great interest.

Blended powder semisolid forming (BPSF) is a new method that meets the aforementioned requirements. This method replaces elemental powder materials with prealloyed ones [17]. BPSF consists of three main stages: 1) the uniform distribution of elemental powders of matrix, 2) mechanical alloying, which raises the elemental state powders' temperature and solid diffusion occurs to produce the alloy, and 3) semisolid compaction which fills the free spaces between the solid particles with liquid phase [18]. The change in the mass fractions of the constituents is a restriction that can be done away by blended powder semisolid forming. BPSF not only includes the benefits of conventional semisolid powder metallurgy, but also alters the amount and size of each element in a compound, provided that the mechanical alloying is sufficiently operated [19]. The various techniques employed and the substantial analyses conducted on the flow behavior of semisolid powders have lead powders toward industrial applications [20].

Composite materials including Al7075 reinforced with Al_2O_3 [18], Al−Cu reinforced with *h*-BN [21], have been fabricated via BPSF. However, to the best of the authors' knowledge, the BPSF of Al7075/B_4C has not been investigated yet. The experimental surveys have introduced weak wetting between matrix and reinforcing particles [22], high energy consumption [23], and formation of undesirable phases [24] as some limitations of available production processes of Al7075/B_4C composites. Despite the existence of some liquid phase in BPSF, the temperature of the process is low; consequently, similar to powder metallurgy route, the formation of undesirable phases is eliminated [18]. Besides, because of the initial placement of reinforcing particles from blending stage, the problem of sedimentation in conventional semisolid formed parts is resolved. Also, post-processing operations such as machining is obviated because the semisolid state methods fabricate near net shape parts [25]. To suggest BPSF as a new method for the fabrication of B_4C reinforced composites is to obviate limitations in liquid, solid and semisolid state methods. So, understanding the role of various matrix/reinforcement size ratios and BPSF process parameters on the properties of the final product is the essential step in the evaluation of the suitability of such composites for industrial applications. Therefore, this work is aimed to develop Al7075/B_4C composites via BPSF.

In this work, elemental aluminum and other constituents of Al7075 were utilized to fabricate B_4C reinforced Al7075 composites by BPSF. The effects of matrix particle size, B_4C volume fraction, and semisolid compaction pressure on the microstructure, physical and mechanical properties were investigated. Also, compositional analysis was performed to determine new phases formed in BPSF of Al7075/B_4C composites.

2 Experimental

2.1 Materials

Three different types of gas atomized Al powder (Khorasan Powder Metallurgy Company) with a particle size of 20 μm (99.96% in purity), 45 μm (99.94% in purity) and 63 μm (99.94% in purity) were used as the base elements for Al7075 blends. The contents of Al7075 alloy elements are given in Table 1. B_4C particles (87% in purity) with average particle size of 45 μm were utilized to reinforce Al7075 alloys. The densities of Al and B_4C powders were 2.80 and 2.51 g/cm^3, respectively.

Table 1 Contents of Al7075 alloy elements (mass fraction, %)

Zn	Mg	Cu	Cr	Mn	Fe	Si	Al
5.5	2.5	1.5	0.23	Trace	Trace	Trace	Bal.

2.2 Fabrication of Al7075/B_4C composites

Three types of Al powder, and one type of B_4C powder were used to fabricate Al7075/B_4C composites and Al7075 alloy samples. Specific amounts of each powder were poured into an ethanol solution, and the solution was placed in a mechanical mixer (IKA's overheard stirrer, RW 47 digital). The speed of the mixer was set to be 100 r/min in all samples. Then, the samples were dried at room temperature. Afterwards, the mechanical alloying was used to blend Al7075 mixture with B_4C particles for 5 h in a planetary ball mill (NARYA-MPM−2*250, Amin-Asia Company) with a transmission ratio of about 3:1 and a sun speed of 200 r/min. The vial and the balls were made of PA and steel, respectively. The volume of the vial was 250 mL. Using balls of 8 and 10 mm in diameter, the ball to powder mass ratio was set to be 10:1. To avoid agglomeration of powder particles during mechanical milling, stearic acid was utilized as a process control agent. The samples were dried in air after mixing; then, 10 g of each mechanically-milled powder was poured into the mold cavity (Fig. 1(b)). Figure 1(a) shows the experimental setup used in the BPSF process. Die material was L316 stainless steel. Compaction setup was placed in furnace (details in Fig. 1(c)). A cold compaction pressure of 200 MPa was applied on samples for 4 min. The heating cycle was then started. Once the sample reached the semisolid temperature range of

Al7075, pressure was applied. Process semisolid temperature was 610 °C in all experiments at which 25% (mass fraction) of Al7075 alloy is liquid. Diffraction scanning calorimeter (Setaram, France) was utilized to obtain liquid fraction versus temperature profile of the alloy (Fig. 2(a)). The samples were kept at this temperature for 30 min. Then, the furnace was turned off, and the pressure was removed. Final parts remained in the furnace for 30 min and, then, were moved to fresh air where they were cooled down to room temperature; finally, some parts of the samples were cut to be analyzed and mechanically tested.

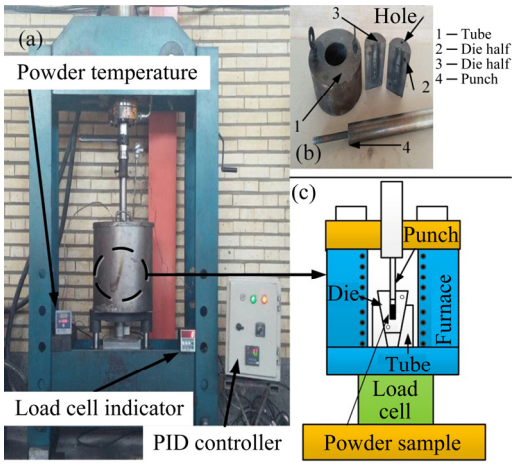

Fig. 1 Experimental setup of BPSF process: (a) Assembled instrument of BPSF; (b) Die components; (c) Details of compaction setup inside furnace

Using thermocouples placed within the powder and on the die surface, the initial powders heating cycle to semisolid state was measured. As illustrated in Fig. 2(b), the furnace temperature was at first set to be 700 °C and kept at this temperature for about 35 min. When the powder temperature reached 610 °C, the temperature of the furnace was set to be 630 °C. After that, temperature difference between the die and the furnace was stable. This heating profile was used in all experiments. In addition to this experiment, to insure the powder temperature gradient during furnace heating, a hole was embedded on the die (Fig. 2(b)). The depth of the hole was equal to the depth of the mold cavity. In experiments, a thermocouple was placed within the hole and the temperature of the bottom of the hole was measured during experiments.

2.3 Design of experiments

Experiments were conducted to investigate the effects of the size and microstructure of the matrix phase, reinforcing volume fraction and the applied compaction pressure on the microstructure, mechanical and physical properties of the samples. The experimental arrays are given in Table 2.

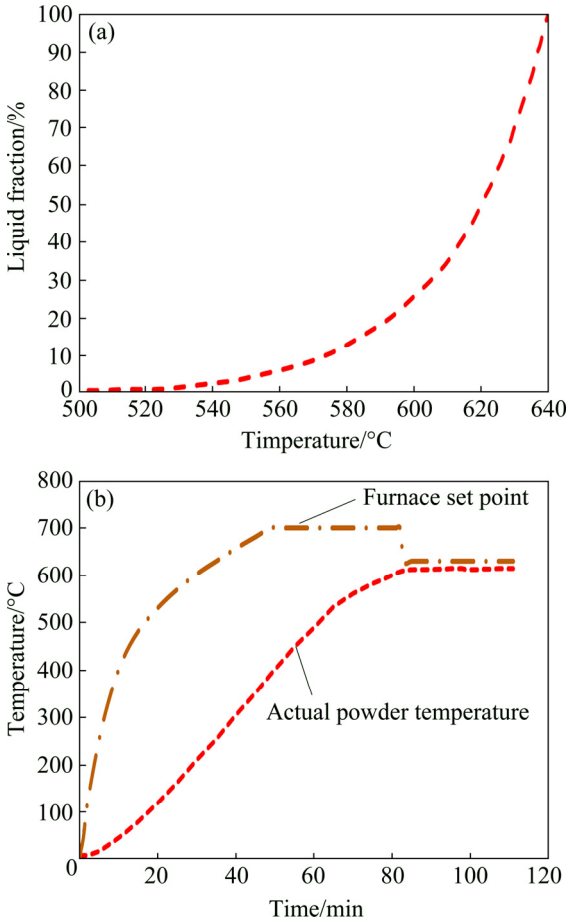

Fig. 2 DSC curve of Al7075 (a) and heating cycle of Al7075 and Al7075/B_4C composites during semisolid compaction (b)

Table 2 Experimental settings

Parameter	Settings
Al matrix particle size/μm	20, 45, 63
B_4C volume fraction/%	5, 10, 20
Semisolid compaction pressure/MPa	50, 100

2.4 Characterization

Polishing of cross sections, normal to the compacted direction, was completed on a standard series of grit papers and diamond polishes. The morphology of the ball-milled powders and microstructure of the polished surface were analyzed using a scanning electron microscope (SEM) (MIRA3 FEG-SEM of Tescan company). The hardness of the cross sections of the samples was determined by micro hardness test using a Vickers indenter (Tukon 1202) at a load of 100 g. The reported values represent the average of 5 measurements on each sample. X-ray diffraction (XRD) analysis was performed on ball-milled and semisolid-compacted samples using a Philips PW1730 diffractometer (40 kV) with Cu K_α radiation (wavelength of 1.54060 nm). Compression tests were performed on samples with 10 mm in diameter and 20 mm in height using universal

hydraulic machine (800 kN) with a speed of 1 mm/min. The bending strength was measured on some samples (20 mm × 6 mm × 5 mm) using a ceramic test system (US MT810). The practical density of the sintered samples was measured by Archimedes' principle coupled with water immersion. The theoretical density was calculated using the density mixture rule [26].

3 Results and discussion

3.1 Powder morphology

In PM routes, mechanical mixing process plays a key role in homogeneous distribution of the reinforcing phase within the matrix, although subsequent processes, such as powder extrusion, can help dispensability of the reinforcing material [27]. The morphology of the powders, matrix and reinforcement, before and after mechanical milling is a key factor in analyzing the mechanical properties of the final bulk products. Figure 3 shows the morphology of the employed matrix and filler powders. Based on their initial size and shape, the powders underwent different deformation mechanisms through the mechanical mixing process. Boron carbide particles had irregularly shaped agglomerates with sharp edges (Fig. 3(a)). As illustrated in Fig. 3(b), 20 μm Al7075 particles had a spherical initial shape. For the

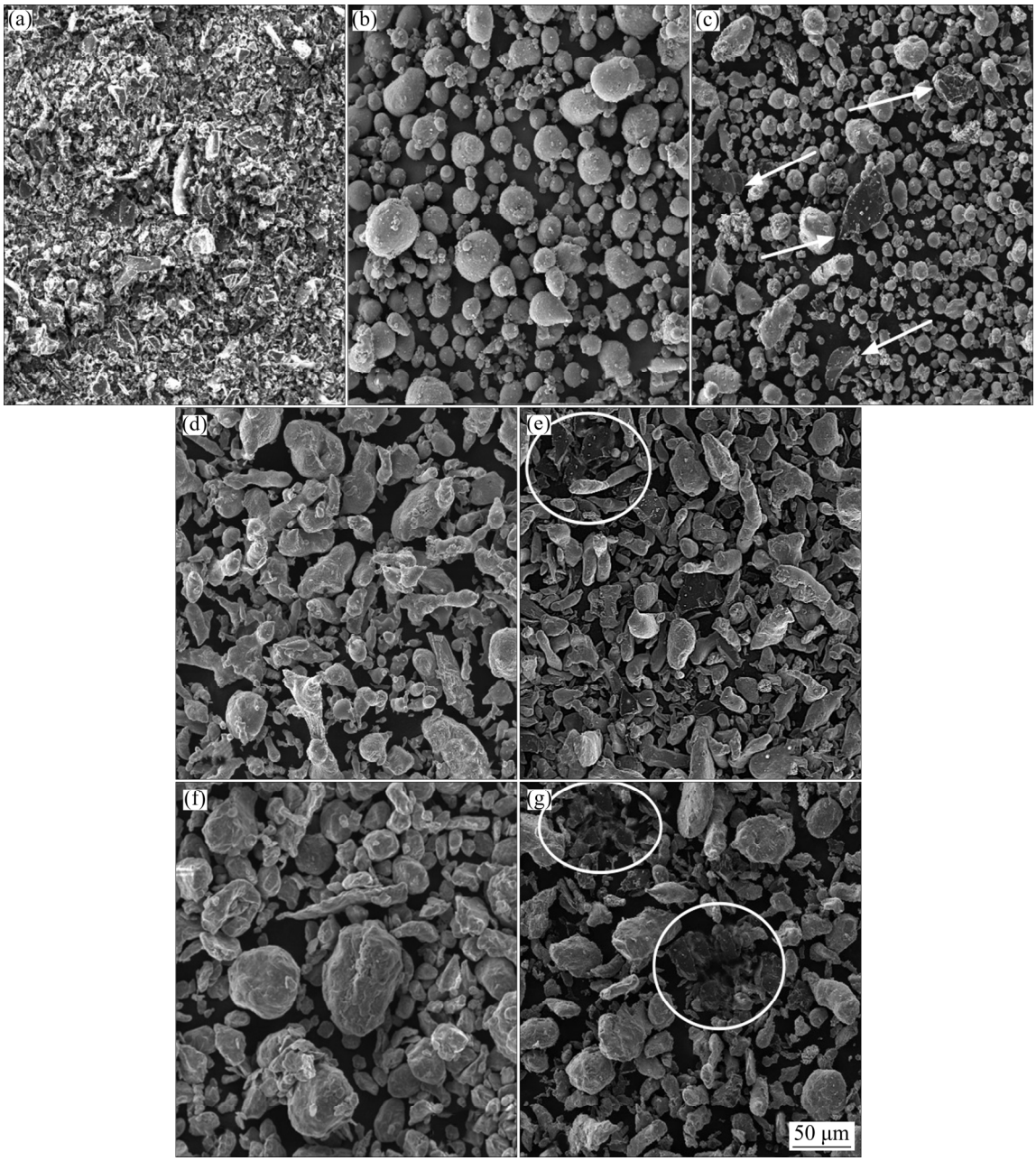

Fig. 3 SEM micrographs illustrating morphology of particles: (a) As-received 45 μm B_4C; (b) As-received 20 μm Al7075; (c) Milled 45 μm B_4C/20 μm Al7075; (d) As-received 45 μm Al7075; (e) Milled 45 μm B_4C/45 μm Al7075; (f) As-received 63 μm Al7075; (g) Milled 45 μm B_4C/63 μm Al7075

combination of 20 μm Al7075 and 45 μm B_4C particles, the distribution of the reinforcement particles within the matrix phase was uniform and matrix particles maintained their initial morphology after milling (Fig. 3(c)). 45 μm Al7075 particles had elliptical shape with soft outer surfaces (Fig. 3(d)). In the mix of these particles with 45 μm B_4C, two different types of uniform and agglomerated regions were observed (Fig. 3(e)). 63 μm Al7075 particles were of near-spherical shape and rough outer surfaces (Fig. 3(f)). Milling process of these particles with 45 μm B_4C resulted in relatively flattened morphology of the matrix particles and local agglomeration of the reinforcing particles (white circles in Fig. 3(g)). When the matrix particle size exceeded the reinforcement particle size, clustering of the reinforcement occurred. This is due to the fact that the reinforcement clusters cannot transfer shear and tensile stresses due to contiguous particulates [28].

3.2 Microstructure

Microstructures of the Al7075/B_4C bulk samples produced by BPSF at different experimental conditions are demonstrated in Fig. 4. Different initial morphology of the powder particles formed distinctive arrangements in the final products. In samples where the size of the matrix particles was smaller than that of the reinforcement particles (i.e., 45 μm B_4C and 20 μm Al7075), the distribution of the reinforcement particles was uniform (Figs. 4(a) and (b)). As shown by white arrows in Fig. 4(a), micro-sized pores existed within the matrix phase particles. This can be attributed to the low compressability of the spherical matrix phase, which resulted in the insufficient bond between the soft phase particles at this level of pressure (50 MPa) [29,30]. Higher pressure of 100 MPa pushed the liquid phase of the Al7075 into the gaps between matrix particles and thus reduced number of voids (Fig. 4(b)). Though relatively uniform distribution of the boron carbide particles was observed for this size ratio in all volume fractions of additions in the present work, reinforcing particles gradually started to aggregately appear in the microstructure, as indicated by white circle in Fig. 4(b), hence, composites with reinforcing volume fractions more than 20% may experience more aggregation.

In the composites containing 5% (volume fraction) of 45 μm reinforcement particles within 45 μm matrix particles (when the sizes of the matrix and the reinforcement particles were closer), the reinforcement

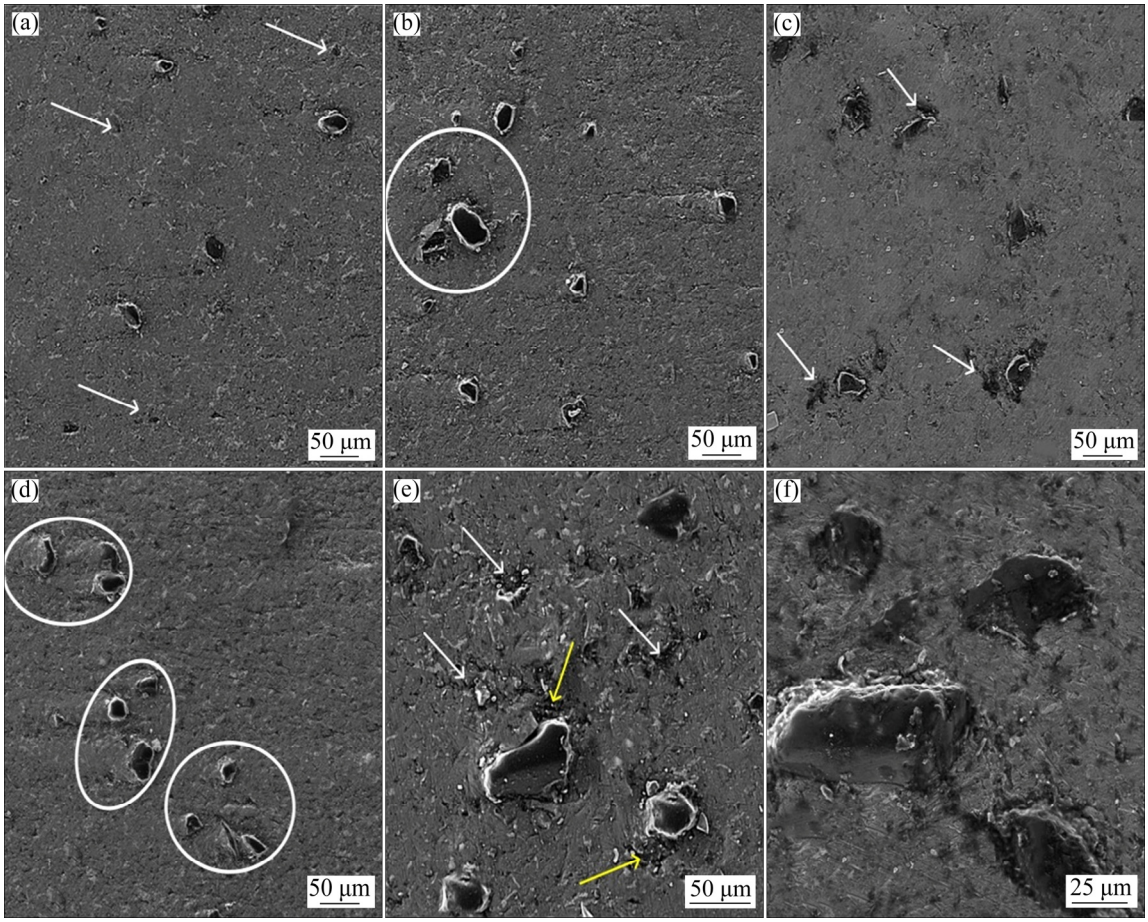

Fig. 4 SEM images of composites with 5% and 20% B_4C under different experimental conditions: (a) 50 MPa, 20 μm Al7075/45 μm B_4C; (b) 100 MPa, 20 μm Al7075/45 μm B_4C; (c) 50 MPa, 45 μm Al7075/45 μm B_4C; (d) 100 MPa, 45 μm Al7075/45 μm B_4C; (e) 50 MPa, 63 μm Al7075/45 μm B_4C; (f) 100 MPa, 63 μm Al7075/45 μm B_4C

particles were uniformly scattered in the microstructure (Fig. 4(c)). In this case, some micro pores, as indicated by white arrows in Fig. 4(c), were observed between the matrix and fillers' interfaces due to the insufficient semisolid compaction pressure of 50 MPa [18]. For this case, the free spaces between matrix particles were completely filled with liquid phase due to the irregular morphology of the matrix particles which facilitated plastic deformation of the matrix particles [29,30]. For the same size particles with 20% (volume fraction) reinforcing addition, boron carbide particles appeared as aggregates within the microstructure (Fig. 4(d)). Since in some regions the reinforcement particles had colonially appeared within the matrix phase in ball milling process (Fig. 3(e)), their microstructural arrangement after compaction was influenced by such a pattern from the blending procedure.

There exists for reinforcement concentration a critical value in PM processed particulate reinforced MMCs [28]. It is possible to uniformly distribute the reinforcement particles in the matrix, given that the volume fraction of the reinforcement is below the aforementioned critical value. On the other hand, if the volume fraction goes beyond this critical value, severe agglomeration takes place. A new method was proposed by SLIPENYUK et al [28]. Through this method, the critical volume fraction of reinforcements could be estimated, and this, in turn, made it feasible to uniformly distribute the reinforcement particles in the Al matrix composites. It was assumed in this model that cubic reinforcement particles (with d-side cube) were uniformly distributed among cubic matrix powder particles (with the cubic side D) in the composites. The matrix particles were hypothesized to be separated from each other by monolayer of reinforcement particles. The particles of matrix alloy (initially cubic) tend to become, after extrusion, rectangular parallelepipeds with dimensions of $(D/\sqrt{\lambda},\ D/\sqrt{\lambda},\ \lambda D)$. The morphology of the particles, however, would undergo no changes. SLIPENYUK's formula, having its foundations on these presuppositions, created the following equation to estimate the critical volume fraction of the fillers:

$$W_{\text{crit}} = \delta\frac{V_{\text{R}}}{V_{\text{M}}+V_{\text{R}}} = \delta\frac{(\frac{D}{\sqrt{\lambda}}+d)\cdot(\frac{D}{\sqrt{\lambda}}+d)\cdot(\lambda D+d)-D^3}{V_{\text{M}}+V_{\text{R}}} = \delta[1-(1+(\frac{d}{D})^3+(\frac{2}{\sqrt{\lambda}}+\lambda)(\frac{d}{D})^2+(\frac{1}{\lambda}+2\sqrt{\lambda})\frac{d}{D})^{-1}] \quad (1)$$

where λ is the extrusion ratio which is set to be 1 in the present work due to the uniaxial compression occurred in BPSF, δ(=0.18) is a constant [28], V_{R} and V_{M} are the volume fractions of the B_4C and Al7075 powders, respectively, and d/D is the ratio of reinforcement/matrix particle sizes.

The results of the calculation of the critical volume fractions based on Eq. (1) for each combination of the matrix and filler are summarized in Table 3. In all the cases, particles with volume fraction higher than 10% are prone to agglomeration. The critical value of 17.47% for the 20 μm Al7075/45 μm B_4C structure affirms that this size ratio of a blend is gradually inclined towards agglomeration, which is consistent with the particle distribution, as indicated by white circle in Fig. 4(b). In the case of the other blends with size ratios of 1.000 and 0.714, composition had experienced agglomeration because the difference between practical values used in this work and critical values based on the SLIPENYUK's model is going to become more, so, microstructures with more agglomerated fillers were accomplished (Figs. 4(d) and (f)).

In the case of 63 μm Al7075 reinforced with 5% (volume fraction) 45 μm B_4C, microstructures (Fig. 4(e)) showed micro-sized free spaces at low compaction pressure of 50 MPa. In this particle size mixing, pores appeared in the interfaces of both matrix particles and matrix−reinforcement. In addition to the low compaction pressure of the process in this condition, the nearly spherical powder morphology of the matrix particles lowered the compressability of the powder compacts [18]. Blending procedure patterns for this combination (Fig. 3(g)), proved final microstructure of the composite. Besides, the critical value calculated from SLIPENYUK's model (Table 3) affirms more tendencies to agglomeration than other two sets of size ratios. Similar to the other size ratios, applying relatively higher pressure of 100 MPa rearranged and disrupted hardened matrix particles and helped them to share more surface areas with surrounding particles, and as a result, liquid phase of Al7075 could flow and fill the gaps [21].

3.3 Density and densification behavior

Table 4 shows the experimental and theoretical density of the composites produced by BPSF. Different spatial arrangements of the particles, matrix and reinforcement, in mechanical alloying and compaction process (Figs. 3 and 4) led to the distinctive densification behaviors. Variations of density as a function of reinforcing volume fractions for samples pressed under 100 MPa are depicted in Fig. 5. Both matrix and reinforcement interface free spaces and small density of the reinforcing powder decreased the density values in composite samples (Fig. 5) [31]. In the case of 20 μm Al7075/45 μm B_4C composites, the large reinforcing

particles were uniformly distributed within the small Al matrix particles (Figs. 4(a) and (b)) and a sufficient degree of wetting was achieved by the liquid phase of the matrix (Fig. 6(a)), so, decreasing trend of the density in this case is related to the lower density of the boron carbide particles compared to the matrix [31].

In the case of 45 μm Al7075/45 μm B_4C composites, however, aggregates of B_4C particles existed from blending stage (Fig. 3(e)) appeared within microstructure in higher reinforcement loading condition (Fig. 4(d)). B_4C agglomerated networks appeared within matrix particles, as indicated schematically in Fig. 6(b), and the liquid phase originated from Al7075 failed to penetrate into the free spaces due to the B_4C strong networks resistance against movement of matrix phase; so, pores were created within the composite structures, which lowered the density.

The lowest density was obtained for 63 μm Al7075/45 μm B_4C composites. In this case, other than agglomerated networks of the reinforcing particles (Fig. 6(c)), the nearly spherical morphology of the matrix particles had negative effect on the densification behavior of the samples [29,30]. Higher compaction pressure of 100 MPa forced the liquid phase to fill gaps within the matrix particles (Fig. 4(f)); still, low density was accomplished for 20% (volume fraction) addition

Table 3 Critical volume fraction of B_4C reinforcement for different particle mixing

Composition No.	Matrix particle size, D/μm	Reinforcement particle size, d/μm	d/D ratio	Reinforcement critical volume fraction/%
1	20	45	2.250	17.47
2	45	45	1.000	16.80
3	63	45	0.714	14.42

Table 4 Density and hardness of blended powder semisolid formed Al7075 alloy samples and Al7075/B_4C composites

Exp. No.	Filler volume fraction/%	Filler particle size/μm	Matrix particle size/μm	Compaction pressure/MPa	Hardness (HV)	Theoretical density/(g·cm^{-3})	Experimental density/(g·cm^{-3})	Relative density/%
1	0	−	20	50	156	2.800	2.680	95.720
2	0	−	20	100	165	2.800	2.733	97.610
3	0	−	45	50	160	2.800	2.711	96.851
4	0	−	45	100	169	2.800	2.760	98.571
5	0	−	63	50	158	2.800	2.683	95.837
6	0	−	63	100	167	2.800	2.741	97.921
5	5	45	20	50	172	2.785	2.649	95.111
6	10	45	20	50	176	2.771	2.634	95.054
7	20	45	20	50	182	2.742	2.641	96.347
8	5	45	20	100	177	2.785	2.748	98.685
9	10	45	20	100	185	2.771	2.727	98.437
10	20	45	20	100	189	2.742	2.679	97.694
11	5	45	45	50	169	2.785	2.698	96.928
12	10	45	45	50	174	2.771	2.666	96.201
13	20	45	45	50	173	2.742	2.619	95.511
14	5	45	45	100	175	2.785	2.724	97.842
15	10	45	45	100	182	2.771	2.707	97.695
16	20	45	45	100	180	2.742	2.643	96.376
17	5	45	63	50	167	2.785	2.661	95.567
18	10	45	63	50	176	2.771	2.644	95.431
19	20	45	63	50	172	2.742	2.598	94.781
20	5	45	63	100	171	2.785	2.701	96.974
21	10	45	63	100	178	2.771	2.680	96.746
22	20	45	63	100	174	2.742	2.622	95.637

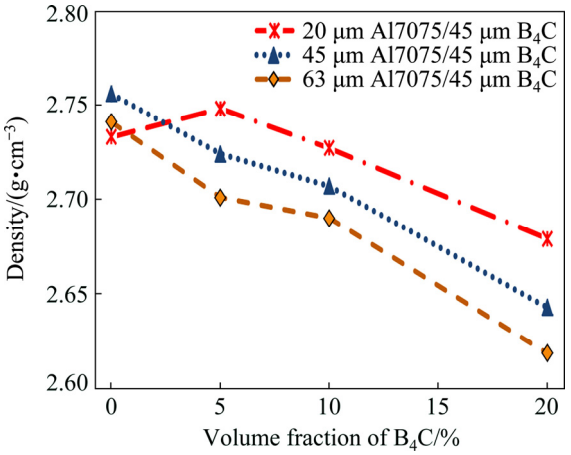

Fig. 5 Practical densities of various Al7075 alloy samples and Al7075/B_4C composites, prepared under 100 MPa, as function of reinforcing volume fraction

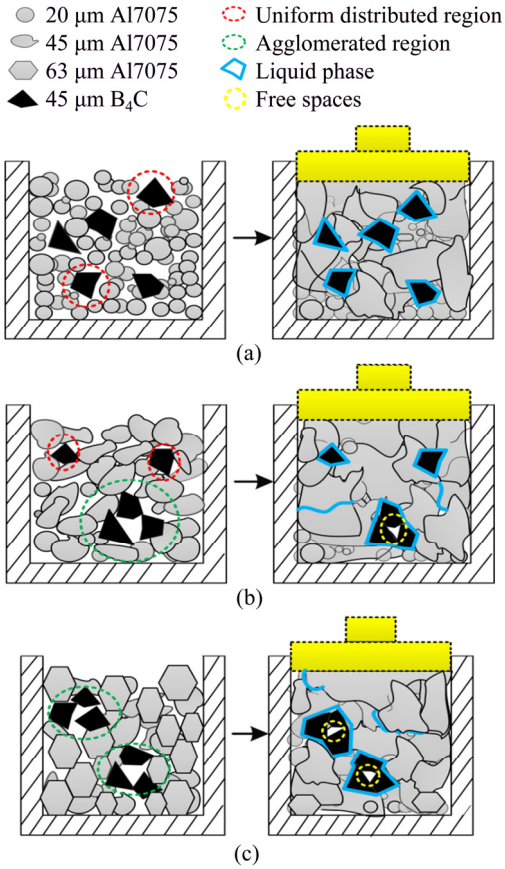

Fig. 6 Schematic illustration of densification behavior during semisolid formation of 20% B_4C reinforced Al7075 matrix composite: (a) 20 μm Al7075/45 μm B_4C; (b) 45 μm Al7075/45 μm B_4C; (c) 63 μm Al7075/45 μm B_4C

due to the non-uniform distribution of the reinforcing particles within matrix phase (Fig. 6(c)).

Comparison of the unreinforced Al7075 compacted parts density which is shown in Fig. 5, revealed that in spherical particles (20 and 63 μm), symmetrical opposite forces appeared in the contact points, which promoted only compressive deformation of particles. An irregular morphology of the particles (45 μm) propitiated the formation of asymmetrically opposite forces in the contact points among particles, which resulted in shear deformation and, consequently, cold-welding of the powder particles. As a consequence, spherical powder was very hard to compact [30]. Low compressibility of the spherical particles lowered relative density of the samples.

3.4 Hardness

Different matrix/reinforcement size ratios in a composite structure affect the final microstructural arrangement [32]. For AMCs, good mechanical performance depends strongly on a homogenous distribution of the reinforcement in the final product. The more the reinforcing particles uniformly dispense within the matrix phase, the more the microstructure resists against indentation. The results of the published surveys showed that uniform distribution of the filler phase resulted in high mechanical properties in BPSF. WU et al [33], in their investigation on high loading condition of Al6061/SiC composite, introduced agglomeration as a main influencer of the composite structures' hardness in semisolid powder forming. Similarly, the hardness in Al7075/Al_2O_3 composites was related to the different combination of matrix and reinforcement sizes and subsequent distribution [18]. The results of the hardness testing for boron carbide reinforced Al7075 indicated that the size of the blended particles, the volume fraction of the reinforcement particles, and the compaction pressure have a significant effect on the hardness of the resultant composite samples. The Vickers micro-hardness values of the composite samples with 5% (volume fraction) B_4C are illustrated in Fig. 7(a). As seen, the composite samples with the larger reinforcement particles, 20 μm Al7075/45 μm B_4C composites, were harder than the samples with other two size ratios. This can be attributed to the uniform distribution of large reinforcement particles, formed during the mechanical blending stage (Fig. 3(c)). This facilitated the load transformation capability from the matrix phase to the hard reinforcement phase and thus resulted in an increased hardness [18].

Generally, other than the hard nature of the boron carbide, hardness in boron carbide reinforced Al7075 composites is in relation to grain boundary strengthening [34], and strengthening from fine particles due to the presence of the boron carbide against movement of dislocations [23]. Provided that the filler is properly imbedded into the matrix phase, above-mentioned mechanisms are activated, so, the first point in the powder metallurgy-based composites is putting insight to dispensability of the particles.

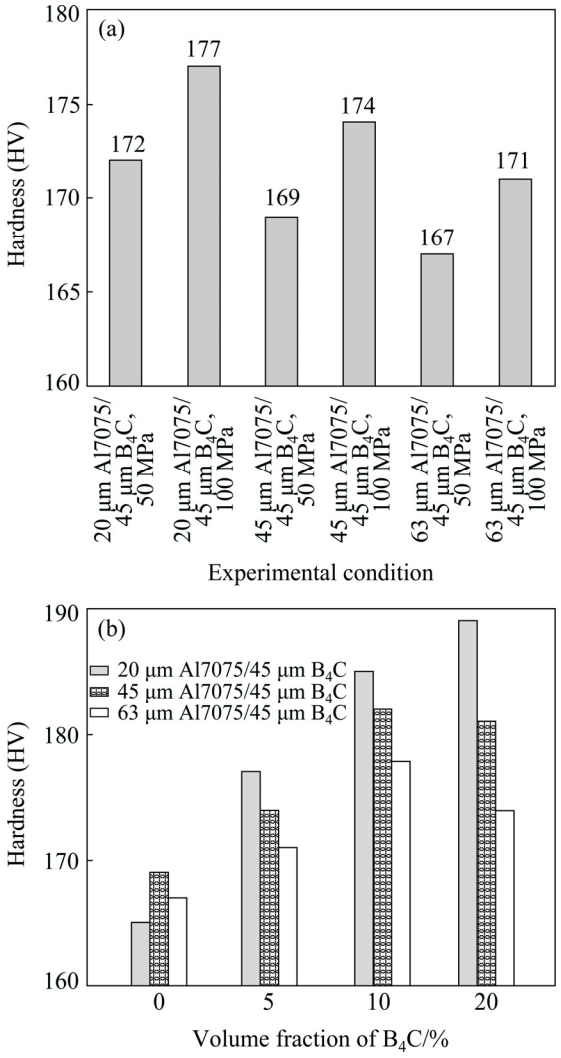

Fig. 7 Vickers micro-hardness test results: (a) Hardness of composite samples with 5% B_4C under different experimental conditions; (b) Hardness versus B_4C content at various combinations of particle sizes and at pressure of 100 MPa

When the compaction pressure of the semisolid forming was increased from 50 to 100 MPa, the hardness of all the samples increased (Fig. 7(a)). Higher pressure forced the liquid phase to move into pore spaces between reinforcement and matrix particles and samples with higher relative density were obtained. So, higher hardness is simply due to the higher relative density obtained with higher pressure [33].

The relationship between the hardness and B_4C content for the composites having various combinations of particle sizes and prepared under 100 MPa compaction pressure is illustrated in Fig. 7(b). As expected, the hardness proportionally increased with the increase of reinforcing volume fraction up to 10%, in all the cases, and a relatively linear relationship was observed. Hardness increase as a result of reinforcement particles addition is attributed to dispersion strengthening. When more reinforcing particles were uniformly distributed within the microstructure, more surface areas of the reinforcing particles were wetted by Al7075 liquid phase and more strong bonds between matrix and reinforcement were distributed throughout final products; consequently, resistant regions against indentation increased. Also, the addition of boron carbide to aluminum matrix increases the number of barriers across dislocations movement and as a result hardness increases [35]. However, adding too much B_4C (20%, volume fraction) slightly decreased the hardness of both 45 μm and 63 μm matrix composites reinforced by 45 μm B_4C particles because of the presence of B_4C agglomerates in these conditions (Figs. 3(d) and (f)).

It is worth noting that the hardness of the unreinforced Al7075 powders (20 μm and 63 μm) with nearly spherical shape was lower than that of 45 μm Al7075 powders with irregular shape. As previously mentioned in Section 3.3, low compressability of the spherical powders lowered the relative density of the composite samples, resulting in the reduced strength of the composites against indentation.

3.5 Compressive and bending strength

Final properties of the metal matrix composites (MMCs) depend on matrix and ceramic properties, bonding between ceramic and matrix, and size and distribution of the ceramic into the aluminum matrix. The compressive strength of the unreinforced Al7075 samples and Al7075/20% B_4C composites with different combinations of the reinforcement and matrix particle size prepared under 100 MPa is illustrated in Fig. 8. Uniform distribution of the reinforcing particles within matrix phase for 20 μm Al7075/45 μm B_4C composites (Figs. 3(c) and 4(b)) and the high compaction pressure affirm the highest amount of compression strength of 336 MPa. B_4C particles exerted more restriction on the plastic flow during deformation, which contributes to the increase in the compressive strength [36]. In the case of 45 μm reinforcement and matrix particles, though better compressibility of the irregular shape particles than spherical ones, B_4C particles had aggregately appeared within matrix particles (Figs. 4(d) and 6(b)). Liquid phase could not completely wet the reinforcing particles' surrounding area due to the resistance of the reinforcing phase networks [18]. So, weak bonding was achieved between matrix and reinforcing particles. This caused to diminish load transfer from the matrix to the stronger ceramic particles and lowered bonding strength of the samples. The critical value of the volume fraction for 63 μm matrix particles with 45 μm reinforcing phase based on SLIPENYUK's model was 14.427% (Table 3), lower than that of two other sets, which demonstrated more tendency to agglomeration (Figs. 3(g) and 4(f)).

The presence of agglomerates within microstructure formed some pores. Existence of pores caused lowered strength [37].

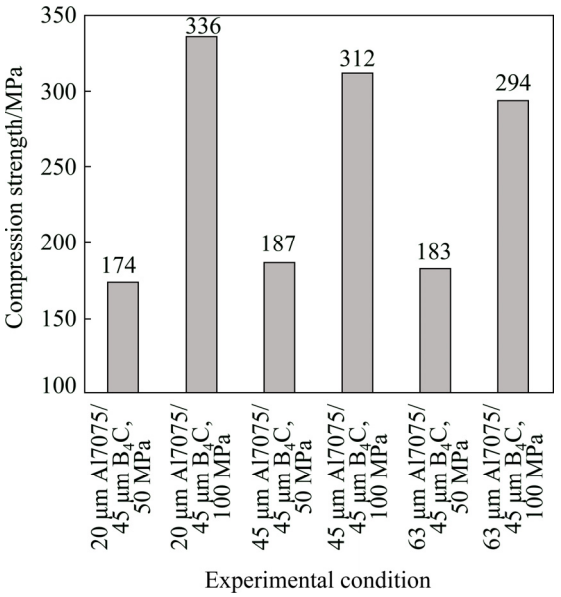

Fig. 8 Compressive strength of different Al7075/20% B_4C composites

To evaluate the reinforcement loading limit in relatively agglomerated composites (45 and 63 μm matrix) and the effect of the reinforcement addition on bending behavior of BPSFed composites, the 63 μm matrix samples with 0%, 5%, 10% and 20% (volume fraction) B_4C reinforcements underwent bending test (Fig. 9). The bending strength of the samples increased to 640 MPa when 10% 45 μm reinforcing particles were added to 63 μm matrix particles. This value is 1.5 times that of the unreinforced Al7075 alloy. Increasing volume fraction of the B_4C to 20% lowered the bending strength. In this loading condition, reinforcing particles appeared as aggregates within matrix (Figs. 3(g) and 4(f)); as a result, unreinforced regions couldn't act as barriers against expansion of cracks through the composite during strength experiment. The same trend has been reported in the characterization of Al7075/B_4C produced by plasma activated sintering [38].

3.6 Compositional analysis

Undesirable phases in B_4C reinforced aluminum alloys reduce the bonding strength [24]. To relate mechanical properties of the composite samples to reactions between Al7075 and B_4C, XRD analysis was performed on 63 μm Al7075/45 μm B_4C composite. XRD spectrum of both mechanically milled and BPSFed 63 μm Al7075 reinforced with 20% (volume fraction) 45 μm B_4C showed Al, B_4C and C peaks (Fig. 10). Similar result has been reported for Al7075/B_4C milled

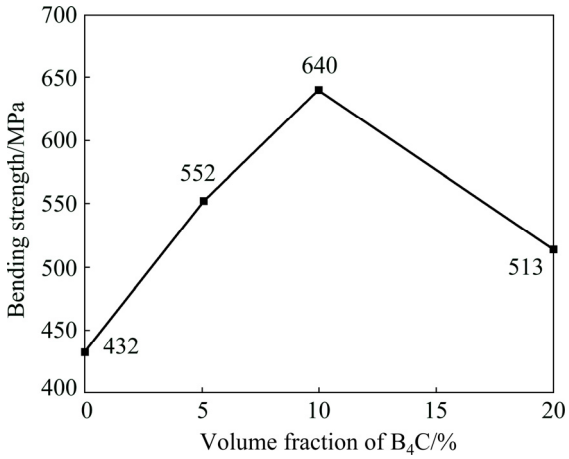

Fig. 9 Bending strength of 63 μm Al7075/45 μm B_4C composites under different reinforcement additions at pressure of 100 MPa

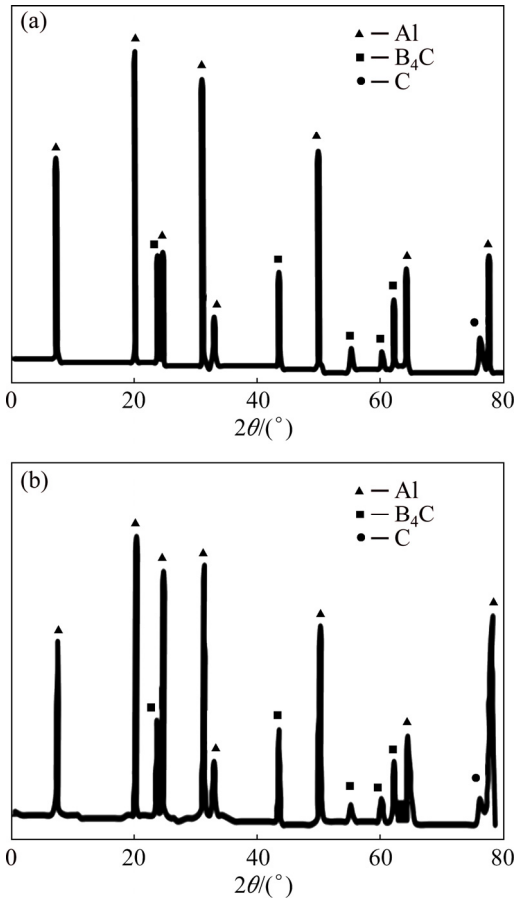

Fig. 10 X-ray diffraction spectra: (a) High energy planetary milled 63 μm Al7075/20% 45 μm B_4C; (b) BPSFed 63 μm Al7075/20% 45 μm B_4C under 100 MPa

powders due to the relatively short duration of the milling [39]. Though undesirable phases observed in liquid state methods [24], in the present work, new phase was not observed. Existence of C peaks in Figs. 10(a) and (b) refers to the as-received state of the B_4C powders. Commercially produced boron carbide is synthesized

using a carbothermal reduction process. This involves carbon reduction of the inexpensive starting material boric acid (H_3BO_3) by heating in an electric heating furnace. The overall carbon reaction can be presented as [40]

$$4H_3BO_3+7C \rightarrow 6CO+6H_2O \quad (2)$$

This reaction proceeds in three steps:

$$4H_3BO_3 \rightarrow 2B_2O_3+6H_2O \quad (3)$$

$$B_2O_3+3CO \rightarrow 2B \quad (4)$$

$$B+C \rightarrow B_4C \quad (5)$$

Complete reaction of carbon is very difficult because the reaction by-product, such as carbon monoxide carries volatile boric species away from the reaction site, breaking the stoichiometry. This results in the final boron carbide containing a considerable amount of free carbon residue [41]. It is concluded from XRD analysis that in the BPSFed 63 μm Al7075/20% of 45 μm B_4C composite, poor mechanical properties is not related to such intermetallic and metallic phases.

4 Conclusions

1) In the compaction of 20 μm Al7075/45 μm B_4C, B_4C particles were uniformly distributed within Al7075 particles. In the case of 45 μm matrix and reinforcing particles, two different regimes were observed: uniformly distributed B_4C particles and agglomerated B_4C areas. 63 μm Al7075/45 μm B_4C particles had more agglomerated regions. In all the cases, reinforcing particles appeared in the microstructure as they were in the mechanical milling stage.

2) The highest hardness of HV 190 was accomplished when the large reinforcing particles (20%, volume fraction) were added to small matrix particles (20 μm). The hardness decreased when the sizes of the matrix and reinforcing phase were closer (i.e., 45 μm Al 7075 and 45 μm B_4C) or the matrix particle sizes was larger than that of the reinforcement (i.e., 63 μm Al7075 and 45 μm B_4C). This behavior was attributed to the uniform distribution of large reinforcing particles within the microstructure.

3) When the matrix phase was not smaller than reinforcing phase (i.e., 45 μm Al7075/45 μm B_4C and 63 μm Al7075/45 μm B_4C), the agglomeration of reinforcing particles appeared between the matrix particles and resisted the liquid phase infiltrating into the free spaces; consequently, the practical density decreased.

4) Increasing reinforcing to 10% (volume fraction) of mixture in 45 μm Al7075/45 μm B_4C and 63 μm Al7075/45 μm B_4C composites improved hardness and bending strength. Adding higher values (20%, volume fraction) lowered mechanical properties of the samples due to the appearance of the agglomerates.

5) Applying more compaction pressure resulted in better liquid phase filling of the empty spaces and thus improved both the density and hardness of the composites.

6) No new phase was created within the samples during mechanical milling and semisolid compaction of 63 μm Al7075/45 μm B_4C composites, and as a result, BPSF in low liquid fractions did not produce brittle phases.

7) The highest compressive strength improvement of about 93% was achieved for 20 μm Al7075 matrix particles with the incorporation of 20% (volume fraction) 45 μm B_4C particles due to the uniform dispersion of the completely wetted reinforcing particles within matrix particles.

Acknowledgements

The authors would like to thank Tabriz Branch, Islamic Azad University for the financial support of this research, which is based on a research project contract.

References

[1] AZIZIEH M, IRANPARAST D, DEZFULI M A G, BALAK Z, KIM H S. Fabrication of Al/Al_2Cu in situ nanocomposite via friction stir processing [J]. Transactions of Nonferrous Metals Society of China, 2017, 27: 779−788.

[2] SIVAKUMAR G, ANANTHI V, RAMANATHAN S. Production and mechanical properties of nano SiC particle reinforced Ti−6Al−4V matrix composite [J]. Transactions of Nonferrous Metals Society of China, 2017, 27: 82−90.

[3] XU Z G, JIANG L T, ZHANG Q, QIAO J, GONG D, WU G H. The design of a novel neutron shielding B_4C/Al composite containing Gd [J]. Materials & Design, 2016, 111: 375−381.

[4] OZER A. The microstructures and mechanical properties of Al−15Si−2.5Cu−0.5Mg/(wt%)B_4C composites produced through hot pressing technique and subjected to hot extrusion [J]. Materials Chemistry and Physics, 2016, 183: 288−296.

[5] SHACKELFORD J F, ALEXANDER W. Materials science and engineering handbook [M]. 3rd ed. Boca Raton: CRC Press Inc., 2000.

[6] KATKAR V A, GUNASEKARAN G, RAO A G, KOLI P M. Effect of the reinforced boron carbide particulate content of AA6061 alloy on formation of the passive film in seawater [J]. Corrosion Science, 2011, 53: 2700−2712.

[7] VIJAYA RAMNATH B, ELANCHEZHIAN C, JAIVIGNESH M, RAJESH S, PARSWAJINAN C, SIDDIQUE AHMED GHIAS A. Evaluation of mechanical properties of aluminium alloy–alumina–boron carbide metal matrix composites [J]. Materials & Design, 2014, 58: 332−338.

[8] POOVAZHAGAN L, KALAICHELVAN K, RAJADURAI A, SENTHILVELAN V. Characterization of hybrid silicon carbide and boron carbide nanoparticles-reinforced aluminum alloy composites [J]. Procedia Engineering, 2013, 64: 681−689.

[9] JIANG J, WANG Y, NIE X, XIAO G. Microstructure evolution of semisolid billet of nano-sized SiC_p/7075 aluminum matrix composite

during partial remelting process [J]. Materials & Design, 2016, 96: 36−43.

[10] HOZIEFA W, TOSCHI S, AHMED M M Z, MORRI A, MAHDY A A, EL-SAYED SELEMAN M M, EL-MAHALLAWI I, CESCHINI L, ATLAM A. Influence of friction stir processing on the microstructure and mechanical properties of a compocast AA2024-Al_2O_3 nanocomposite [J]. Materials & Design, 2016, 106: 273−284.

[11] RAHSEPAR M, JARAHIMOGHADAM H. The influence of multipass friction stir processing on the corrosion behavior and mechanical properties of zircon-reinforced Al metal matrix composites [J]. Materials Science and Engineering A, 2016, 671: 214−220.

[12] JIANG L, WEN H, YANG H, HU T, TOPPING T, ZHANG D, LAVERNIA E J, SCHOENUNG J M. Influence of length-scales on spatial distribution and interfacial characteristics of B_4C in a nanostructured Al matrix [J]. Acta Materialia, 2015, 89: 327−343.

[13] ZEBARJAD S M, SAJJADI S A. Microstructure evaluation of Al−Al_2O_3 composite produced by mechanical alloying method [J]. Materials & Design, 2006, 27: 684−688.

[14] WU Y. Development of novel semisolid powder processing for micromanufacturing [D]. Iowa: Iowa State University, 2009.

[15] SAJJADI S A, EZATPOUR H R, BEYGI H. Microstructure and mechanical properties of Al–Al_2O_3 micro and nano composites fabricated by stir casting [J]. Materials Science and Engineering A, 2011, 528: 8765−8771.

[16] LIOYD D J. Particle reinforced aluminium and magnesium matrix composites [J]. International Materials Reviews, 1994, 39: 1−23.

[17] YASUE K, RADJAI A, MIWA K, SAKAGUCHI Y. Semisolid forming of Al−10mass%Mg alloy by blending of elemental powders [J]. Journal of Materials Science, 2003, 38: 3591−3595.

[18] JAVDANI A, POUYAFAR V, AMELI A, VOLINSKY A A. Blended powder semisolid forming of Al7075/Al_2O_3 composites: Investigation of microstructure and mechanical properties [J]. Materials & Design, 2016, 109: 57−67.

[19] WEN C E, YASUE K, YAMADA Y. Fabrication of TiAl by blended elemental powder semisolid forming [J]. Journal of Materials Science, 2001, 36: 1741−1745.

[20] WU Y, KIM G Y, ANDERSON I E, LOGRASSO T A. Experimental study on viscosity and phase segregation of Al−Si powders in microsemisolid powder forming [J]. Journal of Manufacturing Science and Engineering, 2009, 132: 011003−011007.

[21] CHEN C, GUO L, LUO J, HAO J, GUO Z, VOLINSKY A A. Aluminum powder size and microstructure effects on properties of boron nitride reinforced aluminum matrix composites fabricated by semi-solid powder metallurgy [J]. Materials Science and Engineering A, 2015, 646: 306−314.

[22] WU H, ZENG F, YUAN T, ZHANG F, XIONG X. Wettability of 2519Al on B_4C at 1000−1250 °C and mechanical properties of infiltrated B_4C−2519Al composites [J]. Ceramics International, 2014, 40: 2073−2081.

[23] BARADESWARAN A, ELAYA PERUMAL A. Influence of B_4C on the tribological and mechanical properties of Al7075−B_4C composites [J]. Composites Part B: Engineering, 2013, 54: 146−152.

[24] IBRAHIM M F, AMMAR H R, SAMUEL A M, SOLIMAN M S, SAMUEL F H. On the impact toughness of Al−15 vol.% B_4C metal matrix composites [J]. Composites Part B: Engineering, 2015, 79: 83−94.

[25] MESHKABADI R, FARAJI G, JAVDANI A, POUYAFAR V. Combined effects of ECAP and subsequent heating parameters on semi-solid microstructure of 7075 aluminum alloy [J]. Transactions of Nonferrous Metals Society of China, 2016, 26: 3091−3101.

[26] KOK M. Production and mechanical properties of Al_2O_3 particle-reinforced 2024 aluminium alloy composites [J]. Journal of Materials Processing Technology, 2005, 161: 381−387.

[27] JAIN M K, BHANUPRASAD V V, KAMAT S V, PANDEY A B, VARMA V K, BHAT B V R, MAHAJAN Y R. Production and mechanical properties of Al_2O_3 particle-reinforced 2024 aluminium alloy composites [J]. International Journal of Powder Metallurgy, 1993, 29: 267−275.

[28] SLIPENYUK A, KUPRIN V, MILMAN Y, GONCHARUK V, ECKERT J. Properties of P/M processed particle reinforced metal matrix composites specified by reinforcement concentration and matrix-to-reinforcement particle size ratio [J]. Acta Materialia, 2006, 54: 157−166.

[29] RAZAVI HESABI Z, HAFIZPOUR H R, SIMCHI A. An investigation on the compressibility of aluminum/nano-alumina composite powder prepared by blending and mechanical milling [J]. Materials Science and Engineering A, 2007, 454−455: 89−98.

[30] FOGAGNOLO J B, RUIZ-NAVAS E M, ROBERT M H, TORRALBA J M. The effects of mechanical alloying on the compressibility of aluminium matrix composite powder [J]. Materials Science and Engineering A, 2003, 355: 50−55.

[31] LUO G, WU J, XIONG S, SHEN Q, WU C, ZHANG J. Microstructure and mechanical behavior of AA2024/B_4C composites with a network reinforcement architecture [J]. Journal of Alloys and Compounds, 2017, 701: 554−561.

[32] FATHY A, SADOUN A, ABDELHAMEED M. Effect of matrix/reinforcement particle size ratio (PSR) on the mechanical properties of extruded Al−SiC composites [J]. The International Journal of Advanced Manufacturing Technology, 2014, 73: 1049−1056.

[33] WU Y, KIM G Y, ANDERSON I E, LOGRASSO T A. Fabrication of Al6061 composite with high SiC particle loading by semi-solid powder processing [J]. Acta Materialia, 2010, 58: 4398−4405.

[34] SHIRVANIMOGHADDAM K, KHAYYAM H, ABDIZADEH H, KARBALAEI AKBARI M, PAKSERESHT A H, GHASALI E, NAEBE M. Boron carbide reinforced aluminium matrix composite: Physical, mechanical characterization and mathematical modelling [J]. Materials Science and Engineering A, 2016, 658: 135−149.

[35] KARBALAEI AKBARI M, BAHARVANDI H R, MIRZAEE O. Nano-sized aluminum oxide reinforced commercial casting A356 alloy matrix: Evaluation of hardness, wear resistance and compressive strength focusing on particle distribution in aluminum matrix [J]. Composites Part B: Engineering, 2013, 52: 262−268.

[36] ABDOLLAHI A, ALIZADEH A, BAHARVANDI H R. Dry sliding tribological behavior and mechanical properties of Al2024−5wt.%B_4C nanocomposite produced by mechanical milling and hot extrusion [J]. Materials & Design, 2014, 55: 471−481.

[37] DANDEKAR C R, SHIN Y C. Effect of porosity on the interface behavior of an Al_2O_3–aluminum composite: A molecular dynamics study [J]. Composites Science and Technology, 2011, 71: 350−356.

[38] SHEN Q, WU C, LUO G, FANG P, LI C, WANG Y, ZHANG L. Microstructure and mechanical properties of Al-7075/B_4C composites fabricated by plasma activated sintering [J]. Journal of Alloys and Compounds, 2014, 588: 265−270.

[39] MAJZOOBI G H, ATRIAN A, PIPELZADEH M K. Effect of densification rate on consolidation and properties of Al7075−B_4C composite powder [J]. Powder Metallurgy, 2015, 58: 281−288.

[40] ALIZADEH A, TAHERI-NASSAJ E, EHSANI N. Synthesis of boron carbide powder by a carbothermic reduction method [J]. Journal of the European Ceramic Society, 2003, 24: 3227−3234.

[41] JUNG Choong-hwan, LEE Man-jong, KIM Chan-joong. Preparation of carbon-free B_4C powder from B_2O_3 oxide by carbothermal reduction process [J]. Materials Letters, 2004, 58: 609−614.

混合粉末半固态成形 Al7075/B_4C 复合材料在不同实验条件下的显微组织和力学行为

A. JAVDANI, A. H. DAEI-SORKHABI

Department of Mechanical Engineering, Tabriz Branch, Islamic Azad University, Tabriz, Iran

摘　要：通过混合粉末半固态成形法制备 B_4C 增强铝基复合材料。先将 Al7075 元素粉末在机械搅拌状态下逐渐添加到酒精溶液中，然后通过高能球磨将 Al7075 元素粉末与 B_4C 颗粒混合，最后将 Al7075/B_4C 混合粉末在半固体状态下冷压成型。研究基体颗粒尺寸(20、45 和 63 μm)、增强相的体积分数(5%、10%和 20%)和半固态压制压力(50 和 100 MPa)对复合材料的形貌、显微组织、密度、硬度、压缩强度和抗弯强度的影响。实验结果表明，当大的 B_4C 颗粒(45 μm)分布在小的基体相颗粒(20 μm)中时，材料的显微组织最均匀。基体颗粒尺寸大于增强相颗粒尺寸的复合材料中团聚量大于 10%(体积分数)。团聚区域的液相难以渗透到孔隙中，降低复合材料的密度和强度。采用 20 μm Al7075 和 20%(体积分数)45 μm B_4C 粉末在 100 MPa 下压制的复合材料表现出最高的硬度值(HV 190)和抗压强度(336 MPa)

关键词：混合粉末；机械合金化；半固态成形；B_4C；铝基复合材料

(Edited by Bing YANG)